ENVIRONMENTAL RESEARCH
LETTERS

LETTER • OPEN ACCESS

Relationship between circum-Arctic atmospheric wave patterns and large-scale wildfires in boreal summer

ENVIRONMENTAL RESEARCH
LETTERS

LETTER

Relationship between circum-Arctic atmospheric wave patterns and large-scale wildfires in boreal summer

Teppei J Yasunari[1,2,3,*], **Hisashi Nakamura**[4], **Kyu-Myong Kim**[5], **Nakbin Choi**[6], **Myong-In Lee**[6], **Yoshihiro Tachibana**[7] and **Arlindo M da Silva**[5]

[1] Arctic Research Center, Hokkaido University, N21W11, Kita-ku, Sapporo, Hokkaido 001-0021, Japan
[2] Global Station for Arctic Research, GI-CoRE, Hokkaido University, N21W11, Kita-ku, Sapporo, Hokkaido 001-0021, Japan
[3] Center for Natural Hazards Research, Hokkaido University, N9W9, Kita-ku, Sapporo, Hokkaido 060-8589, Japan
[4] Research Center for Advanced Science and Technology, The University of Tokyo, 4-6-1 Komaba, Meguro-ku, Tokyo 153-8904, Japan
[5] NASA Goddard Space Flight Center, 8800 Greenbelt Road, Greenbelt, MD 20771, United States of America
[6] Ulsan National Institute of Science and Technology, 50 UNIST-gil, Eonyang-eup, Ulju-gun, Ulsan 44919, Republic of Korea
[7] Faculty of Bioresources, Mie University, 1577 Kurimamachiya-cho, Tsu, Mie 514-8507, Japan
* Author to whom any correspondence should be addressed.

E-mail: t.j.yasunari@arc.hokudai.ac.jp

Keywords: wildfire, aerosol, $PM_{2.5}$, summer, Arctic, climate pattern, atmospheric circulation

Supplementary material for this article is available online

OPEN ACCESS

RECEIVED
12 October 2020

REVISED
9 March 2021

ACCEPTED FOR PUBLICATION
14 April 2021

PUBLISHED
17 May 2021

Abstract

Long-term assessment of severe wildfires and associated air pollution and related climate patterns in and around the Arctic is essential for assessing healthy human life status. To examine the relationships, we analyzed the National Aeronautics and Space Administration (NASA) modern-era retrospective analysis for research and applications, version 2 (MERRA-2). Our investigation based on this state-of-the-art atmospheric reanalysis data reveals that 13 out of the 20 months with the highest $PM_{2.5}$ (corresponding to the highly elevated organic carbon in the particulate organic matter [POM] form) monthly mean mass concentration over the Arctic for 2003–2017 were all in summer (July and August), during which POM of $\geqslant 0.5\ \mu g\ m^{-3}$ and $PM_{2.5}$ were positively correlated. This correlation suggests that high $PM_{2.5}$ in the Arctic is linked to large wildfire contributions and characterized by significant anticyclonic anomalies (i.e. clockwise atmospheric circulation) with anomalous surface warmth and drier conditions over Siberia and subpolar North America, in addition to Europe. A similar climate pattern was also identified through an independent regression analysis for the July and August mean data between the same atmospheric variables and the sign-reversed Scandinavian pattern index. We named this pattern of recent atmospheric circulation anomalies the circum-Arctic wave (CAW) pattern as a manifestation of eastward group-velocity propagation of stationary Rossby waves (i.e. large-scale atmospheric waves). The CAW induces concomitant development of warm anticyclonic anomalies over Europe, Siberia, Alaska, and Canada, as observed in late June 2019. Surprisingly, the extended regression analysis of the 1980–2017 period revealed that the CAW pattern was not prominent before 2003. Understanding the CAW pattern under future climate change and global warming would lead to better prediction of co-occurrences of European heatwaves and large-scale wildfires with air pollution over Siberia, Alaska, and Canada in and around the Arctic in summer.

1. Introduction

Global concern over wildfires has increased under the ongoing global warming (e.g. Running 2006, Jolly *et al* 2015, Veira *et al* 2016). In two recent years (2019 and 2020), unprecedented wildfires occurred in the Arctic and its vicinity (Witze 2020). During June and July 2019, European heatwaves coincided with large-scale wildfires over Siberia and Alaska (Nature 2019). Based on atmospheric and climate data provided by the Tokyo Climate Center (WMO regional climate center in RA II), large areas of the extratropical Northern Hemisphere, including Europe, Siberia, and Alaska, were suffered from

marked co-occurrences of extremely high temperature during June and August 2019 (https://ds.data.jma.go.jp/tcc/tcc/products/climate/seasonal/seasonal_201906201908e.html) with heatwaves over Europe during June and July (https://ds.data.jma.go.jp/tcc/tcc/products/climate/annual/annual_2019e.html). Severe and extensive wildfires across Alaska in June and July 2019 (see the satellite image at NASA's worldview for 9 July 2019, at: https://go.nasa.gov/3n6PlUq) and Siberia (www.nasa.gov/image-feature/goddard/2019/siberian-smoke-heading-towards-us-and-canada) also emitted air pollutants that were transported into distant areas. Characterized by atmospheric blacking, the Siberian wildfire in the summer of 2019 caused extensive air pollution, including $PM_{2.5,}$ which exceeded the 2011–2019 average values (Bondur *et al* 2020). It has been reported that wildfires in and around Siberia have significant impacts not only on nearby areas but also on remote locations, such as Hokkaido in Japan, which has recorded considerable $PM_{2.5}$ increases (Ikeda and Tanimoto 2015, Yasunari *et al* 2018), and the Arctic (Sitnov *et al* 2020). The above studies suggest meaningful connections among wildfires, aerosols (air pollution), and climate patterns in and around the Arctic region in recent years.

Aerosols over the Arctic region contribute to the so-called Arctic haze (i.e. haze typically seen in spring in the Arctic; Shaw 1995, Quinn *et al* 2007) and affect cloud properties and radiative forcing (Zhao and Garrett 2015). Fractions of carbonaceous aerosols such as black carbon (BC) and organic carbon (OC) can increase owing to wildfires emissions (e.g. Bond *et al* 2004, Wang *et al* 2011, Noguchi *et al* 2015). Another consequence of wildfires is the snow-darkening effect (SDE), which is due to reductions in snow albedo caused by the depositions of light-absorbing aerosols such as BC, OC, and dust (Warren and Wiscombe 1980, Flanner *et al* 2007, 2009, Yasunari *et al* 2010, 2011, Aoki *et al* 2011, Yasunari *et al* 2013, 2014, 2015, Qian *et al* 2015, Lau *et al* 2018, Hock *et al* 2019). Solar forcing by SDE due to post-wildfires has increased in the western US burned forests since 1999 (Gleason *et al* 2019). A recent study revealed that surface melting on the Greenland ice sheet is accelerated during warmer-than-normal summers because of high temperatures and increased BC deposition from wildfires (Keegan *et al* 2014). Therefore, in addition to the essential connections with climate patterns, wildfire-generated aerosols are also of significant concern for climate and snow-darkening interactions.

However, many studies have often focused on individual aerosol constituents that make up $PM_{2.5}$, rather than assessments of comprehensive air pollution (e.g. Sharma *et al* 2004, Eleftheriadis *et al* 2009, Hegg *et al* 2009, Wang *et al* 2011, Yttri *et al* 2014) with a few $PM_{2.5}$ studies in and around the Arctic (Tran and Mölders 2011). Therefore, there is still a lack of statistical research on air pollution, specifically on $PM_{2.5}$, and capturing long-term variability in $PM_{2.5}$ in the Arctic has thus far been difficult in the absence of continuous and extensive $PM_{2.5}$ measurements. Our understanding of long-term $PM_{2.5}$ variation, air quality in the Arctic and its surrounding areas, and their linkage to variations in climatic conditions, such as anomalous atmospheric circulation, is therefore still limited.

Recently, the National Aeronautics and Space Administration (NASA) produced MERRA-2 (Modern-Era Retrospective analysis for Research and Applications, Version 2), a long-term global reanalysis dataset for atmospheric and other conditions such as land and ocean (Bosilovich *et al* 2015). The best quality aerosol-related variables since 2003 in MERRA-2 are available because the most available satellite measurements were merged into the modeled data for this period (Randles *et al* 2017). We, therefore, utilize the MERRA-2 reanalysis data in this study.

Thus far, case studies for Siberian wildfires and associated air pollution in and around the Arctic have been reported (Ikeda and Tanimoto 2015, Yasunari *et al* 2018, Sitnov *et al* 2020). However, a number of questions remained unanswered. To address this knowledge gap, we focused on three key factors in this study: (a) statistical relationships among wildfires, $PM_{2.5}$, and wildfire-related aerosols, especially under high air pollution (i.e. $PM_{2.5}$) conditions, (b) identifying the dominant climate pattern under high $PM_{2.5}$ conditions in the Arctic, and (c) identifying whether this pattern has occurred only in recent years. The state-of-the-art MERRA-2 reanalysis data allowed us to reveal the relationships among wildfires, aerosols (air pollution), and climate patterns in and around the Arctic. The outcome of this study provides a resource to aid in making better forecasts in future studies.

2. Data and methods

2.1. Data

To examine recent temporal variations of air pollutants in the Arctic, we used the monthly MERRA-2 reanalysis data from January 2003 to December 2017 (15 years) for the global atmosphere based on the GEOS-5 model (Rienecker *et al* 2008), including the data assimilation with observations since 1980 (Bosilovich *et al* 2015, Randles *et al* 2017; https://gmao.gsfc.nasa.gov/reanalysis/MERRA-2/). The MERRA-2 atmospheric data from 1980 to 2017 was also used for some additional analysis. The advantage of using MERRA-2 is that observed aerosol optical depth (AOD) data from satellites and ground-based measurements (AERONET) are assimilated (Randles *et al* 2017). When

observed AOD data are available, aerosol data simulated in the GEOS-5 model are modified to reflect the observations (Randles *et al* 2017). The best aerosol quality with lower bias was available in MERRA-2 from 2003 compared to that before 2003 (figure 5 of Randles *et al* 2017). MERRA-2 uses the monthly-mean quick fire emissions dataset (QFED) emissions (Darmenov and Da Silva 2015) up to 2010 and daily QFED emissions afterward. While daily biomass burning (BB) emissions are critical for capturing day-to-day BB emission variability, the switch to daily BB emissions in 2010 does not introduce any long-term trends because the same monthly-mean emissions were used before and after 2010. Notice that despite the fact that monthly mean BB emissions were used prior to 2010, MERRA-2 can still capture daily variability in BB aerosols due to the three-hourly assimilation of aerosol data. Therefore, the switch to daily QFED emissions in 2010 should have minimal impacts on the analysis presented in this study. In the GEOS-5 model, the original air pollutants (i.e. aerosols) are simulated with the goddard chemistry aerosol radiation and transport (GOCART) module (Chin *et al* 2000, Ginoux *et al* 2001, Chin *et al* 2002). In GOCART, OC is treated as Particulate Organic Matter (POM = 1.4 × OC; Colarco *et al* 2010). This POM (OC in MERRA-2) is a good indicator of air pollution from wildfires (e.g. Yasunari *et al* 2018). The MERRA-2 aerosols have been validated regionally and globally in recent studies (e.g. Buchard *et al* 2017, Yasunari *et al* 2017, 2018, He *et al* 2019, Sun *et al* 2019, Gueymard and Yang 2020, Ma *et al* 2020). Besides, a case study for the Siberian wildfire in 2016 using MERRA-2, BC revealed long-range transport of air pollution to the Arctic (Sitnov *et al* 2020), which further validated the usefulness of the MERRA-2 data in/around the Arctic region.

We also used MODIS (moderate resolution imaging spectroradiometer) fire pixel counts (FPCs) retrieved by the Aqua satellite (available at: https://feer.gsfc.nasa.gov/) to construct composites for 13 high $PM_{2.5}$ summer months. Monthly total FPCs aggregated at 1° by 1° both in latitude and longitude are used to discuss a potential source of POM.

For our regression analysis, a known climate index of the Scandinavian pattern (www.cpc.ncep.noaa.gov/data/teledoc/scand.shtml) was used; it was originally defined as the Eurasia type 1 pattern by Barnston and Livezey (1987).

2.2. Analytical techniques and statistics

In this study, $PM_{2.5}$ was calculated from the five MERRA-2 aerosol types in the $PM_{2.5}$ size-dust, sulfate, BC, OC (i.e. POM), and sea salt—by the method (equation (1)) of Buchard *et al* (2016), in which sulfate is assumed to be ammonium sulfate. Monthly-mean values of area-averaged $PM_{2.5}$ within the Arctic circle (at 66.56°N) were computed for 15 years (2003–2017) before choosing the 20 highest $PM_{2.5}$ months. Of which, 13, 5, and 2 months were found in summer (July 2003, August 2003, July 2004, July 2005, July 2006, July 2009, August 2009, July 2012, August 2012, August 2013, July 2014, July 2015, and August 2017), winter (January 2009, December 2011, January 2012, December 2013, and February 2015), and fall (September 2003 and September 2014), respectively (figure 1). Thus, the remainder of the study focused on the summer months. These 13 summer months were then compared with the other 17 summer months (July and August) with the lower $PM_{2.5}$ levels through composite analysis shown later. Welch's t-test (Welch 1938) was used to assess the significant mean differences in the composites. Most composites adopted a two-sided t-test for rejecting the null hypothesis, except for those presented in SI figure S2 and SI table S1 (see supplementary information: SI (available online at stacks.iop.org/ERL/16/064009/mmedia)). For these SI materials, we only would like to verify whether the $PM_{2.5}$ and aerosol mass concentrations over Siberia, Alaska, and Canada for the high $PM_{2.5}$ months in the Arctic are higher than those for the other months. Therefore, we only focused on the positive (i.e. increase) difference and thus used a one-sided t-test for them (i.e. under the alternative hypothesis).

The climate pattern's essential dynamic processes can be illustrated with a particular form of a Rossby wave-activity flux (WAF) (Takaya and Nakamura 2001), parallel to the group velocity of stationary Rossby waves (i.e. large-scale atmospheric waves). According to the linear theory, the flux magnitude is proportional to the squared wave amplitude and the eastward group velocity. The latter is proportional to the background westerly wind speed. The WAF of Takaya and Nakamura (2001) was calculated with the modified script based on the GrADS script for WAF (http://www.atmos.rcast.u-tokyo.ac.jp/nishii/programs/index.html).

3. Results

3.1. Characteristics of $PM_{2.5}$ and aerosols, and their relationships with wildfire

Here, we investigate monthly $PM_{2.5}$ variations during 2003–2017 by selecting 20 months with the worst air quality in the Arctic region. From the area-mean data over the Arctic for 2003–2017 (figure 1), the fractions of dust, ammonium sulfate, sea salt, BC, and OC (POM; hereafter called POM; proportional to OC in MERRA-2: see section 2) are about 2.7%–42.5%, 9.5%–37.5%, 16.7%–73.1%, 0.5%–2.8%, and 1.5%–58.0% of the monthly mean Arctic $PM_{2.5}$, respectively. Generally, the dust contribution tends to be smaller in summer and fall but more prominent in spring. Sulfate aerosols are also smaller in summer. Meanwhile, BC and POM peaked during summer, with the summer fractions reaching 1.0%–2.8% and 13.8%–58.0%, respectively. These

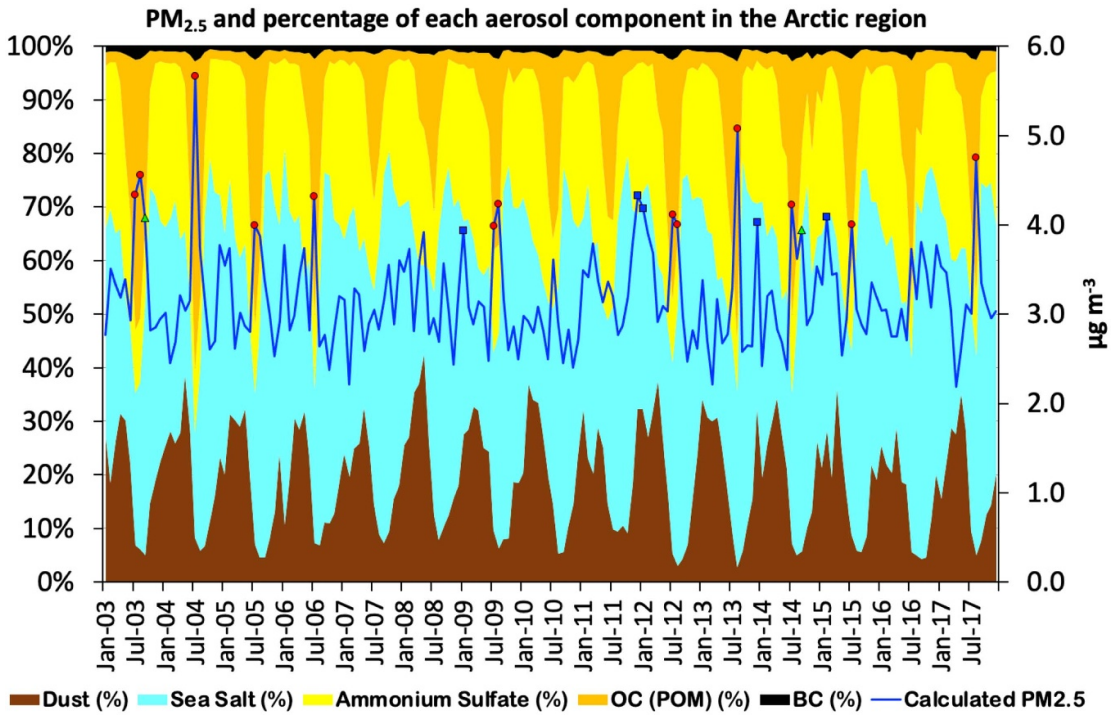

Figure 1. Time evolution of monthly-mean $PM_{2.5}$ concentrations ($\mu g\ m^{-3}$) (right) in the Arctic region and the fractional contributions in percentage (left) of individual aerosol species between 2003 and 2017 based on MERRA-2 data. Red circles, blue squares, and green triangles represent summer, winter, and fall, respectively, covering the 20 months of worst air quality (highest $PM_{2.5}$) in the Arctic. Individual aerosol species include dust, sea salt, ammonium sulfate, (OC; POM), and BC, as detailed in the bottom legend.

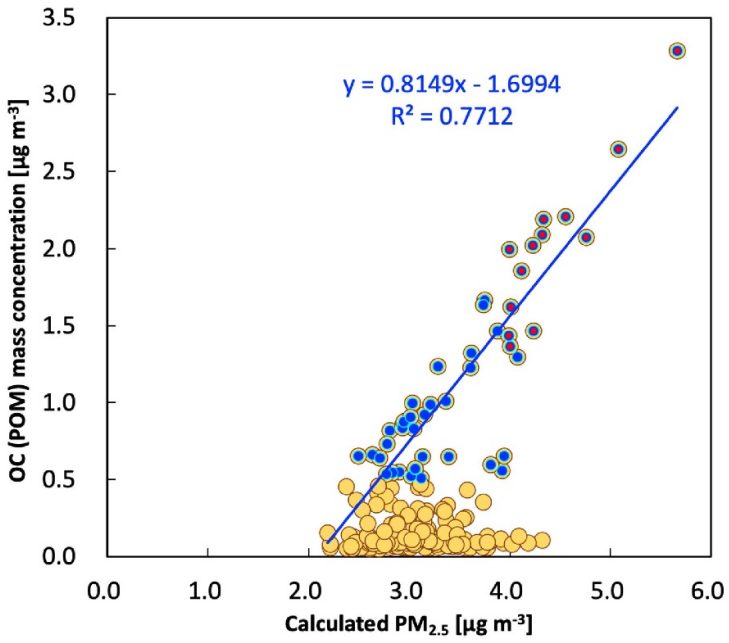

Figure 2. Comparison of calculated MERRA-2 $PM_{2.5}$ and organic carbon (OC; particulate organic matter [POM]) mass concentration in the Arctic from 2003 to 2017. All data are monthly mean values averaged within the Arctic. Light orange circles denote all the data during the period. Blue circles indicate the monthly mean OC (POM) mass concentrations equal to or higher than 0.5 $\mu g\ m^{-3}$. Red circles represent the 13 summer months (July and August) among the 20 months with the highest $PM_{2.5}$ in the Arctic (see figure 1 and section 2.2). The blue line is the linear regression for the blue circle data with its equation and R^2 value.

findings imply a common emission source in summer. Sea salt markedly increases in fall but decreases to a minimum, mainly in spring; its fraction never goes below approximately 16.7%, and the minimum contribution is higher than the other aerosol constituents.

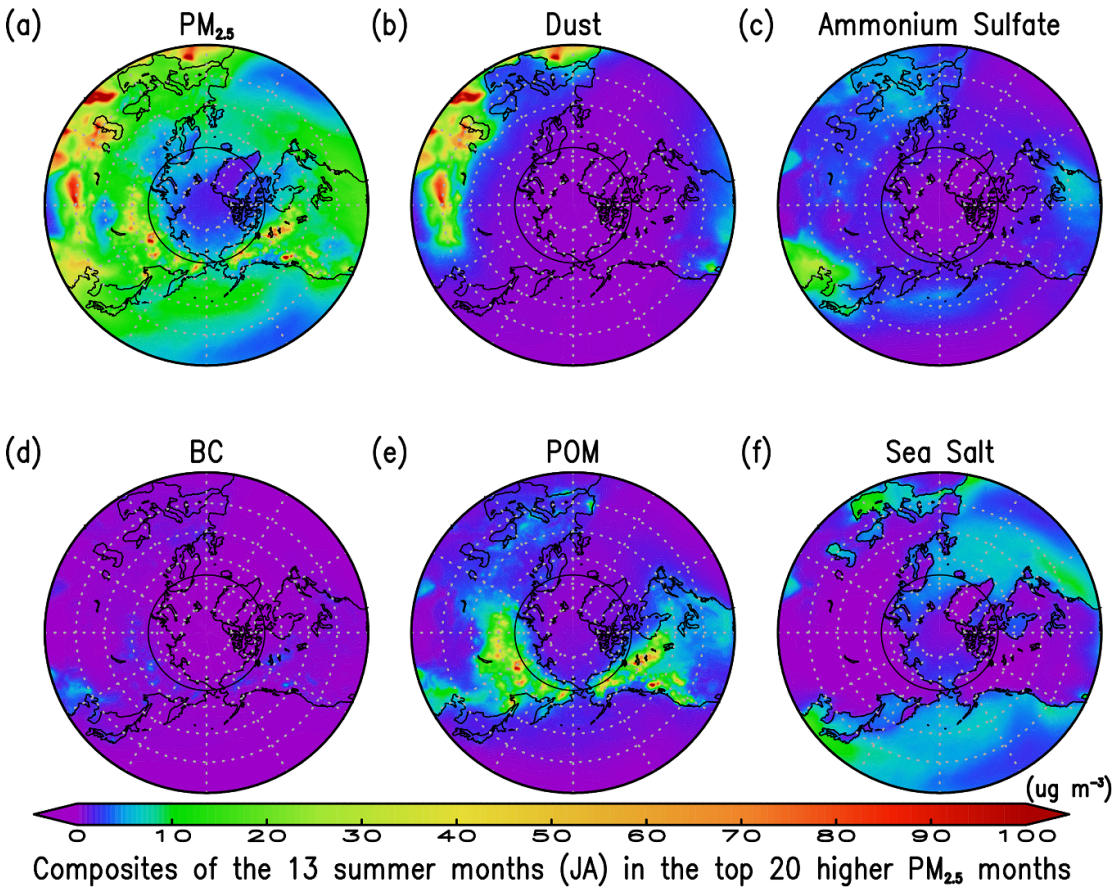

Figure 3. Composites of (a) $PM_{2.5}$ levels for the 13 summer months (July and August) among the 20 months with the highest $PM_{2.5}$ between 2003 and 2017, and the corresponding mass concentrations of (b) dust, (c) ammonium sulfate, (d) BC, (e) POM (see section 2.1), and (f) sea salt. All the units are in $\mu g\ m^{-3}$.

Of the 20 months of the worst air quality based on $PM_{2.5}$, 13 months were in summer (figure 1). These 13 significantly high $PM_{2.5}$ months in summer also correspond to higher POM months for 2003–2017 (figure 2). When the Arctic-averaged monthly-mean POM is not less than 0.5 $\mu g\ m^{-3}$, POM and $PM_{2.5}$ were well explained by its strong linear relationship ($R^2 = 0.77$). Those 13 high $PM_{2.5}$ months in the Arctic summer were also characterized by regionally high POM (figure 3(a)). The POM mass concentrations were greater over Siberia, Alaska, and Canada (figure 3(e)), where wildfires were very active (figure 4). The POM increased significantly in the 13 summer months (July and August) in Siberia and Canada compared with the other July and August months, where increased BC was also prominent (SI figures S1 and S2; SI table S1). The POM increase in Alaska was significant only in July (SI table S1). Those results indicate that the 13 highest $PM_{2.5}$ months in summer (July and August) in the Arctic in 2003–2017 were also higher POM months due to active wildfires over Siberia and subpolar North America in and around the Arctic. Also, the POM increase tended to be accompanied by BC increases from the same areas (figure 3(d)).

3.2. Summer climate pattern under high $PM_{2.5}$ conditions in the Arctic

During the 13 highest $PM_{2.5}$ months in summer (i.e. July and August), significant anticyclonic anomalies (i.e. clockwise atmospheric circulation) from the lower (850 hPa) to mid-troposphere (500 hPa) were identified (figures 5(b) and (c)) over central Siberia and western Canada. The local $PM_{2.5}$ and POM mass concentrations over the regions were significantly high (figures 3(a), (e); SI figures S1 and S2; SI table S1) owing to active wildfires (figure 4). These anticyclonic anomalies tend to accompany anomalous high surface air temperatures (figure 5(a)) that are significant over Siberia and Canada in July and August, as well as significantly drier conditions over Siberia, Alaska, and Canada (SI figure S3). The anomaly pattern in figure 5 also resembles the warm anticyclonic anomalies observed over western Europe, central Siberia, Alaska, and Canada in late June 2019 (SI figure S4).

Figure 6 shows WAF in the atmosphere evaluated from the composite anomaly fields for the 13 summer months and their differences in geostrophic stream functions (from geopotential height) with the composite of horizontal winds for the 17 other summer months at 500 hPa. The warm anticyclonic anomalies

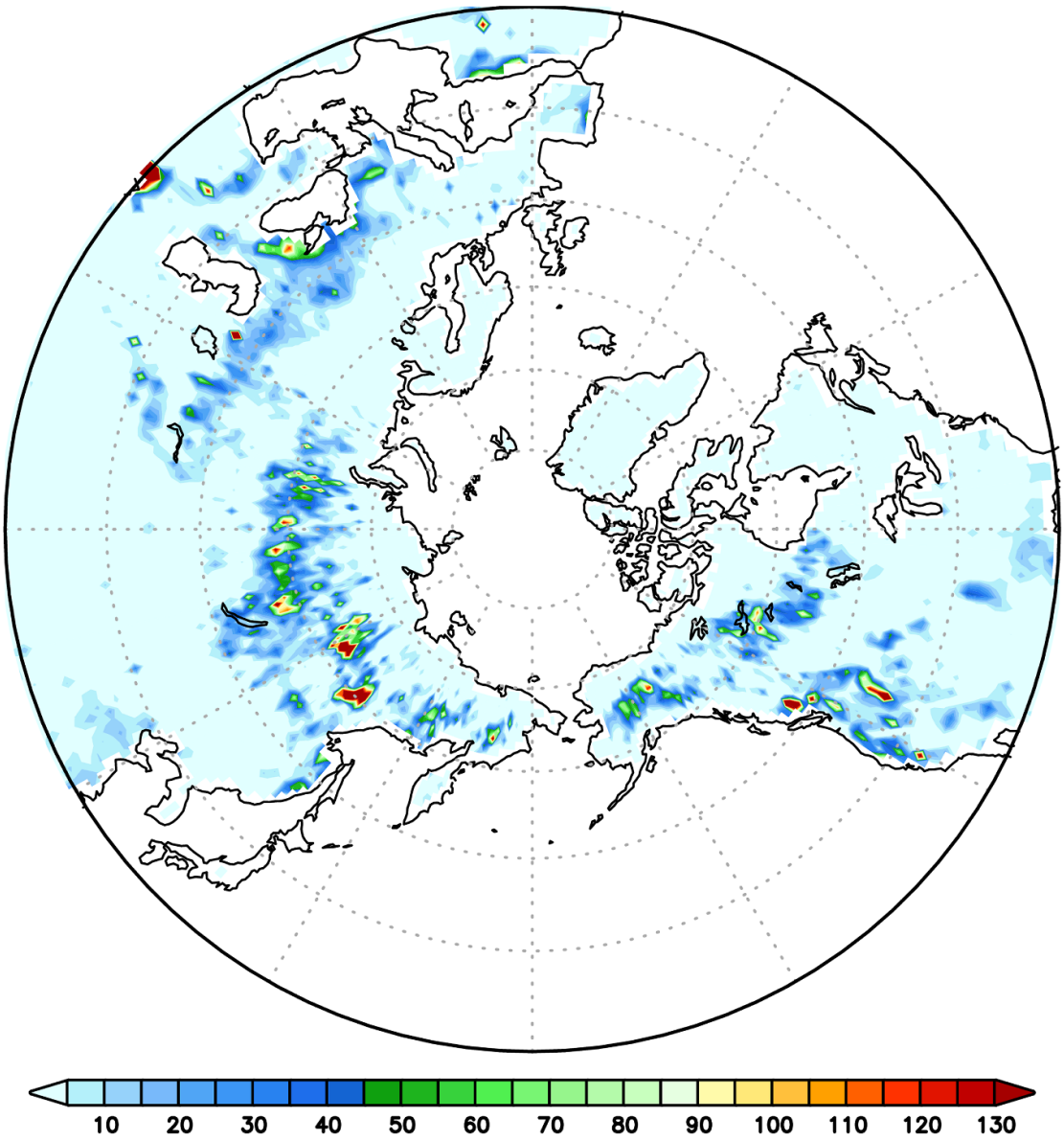

Figure 4. Composite of monthly mean MODIS FPCs (unit: count per 1° latitude × 1° longitude grid) retrieved by the Aqua satellite (available at: https://feer.gsfc.nasa.gov/) for the 13 summer months (July and August) with the highest $PM_{2.5}$ concentrations in the Arctic.

are accompanied by two eastward-developing Rossby wave trains along the westerly jet stream, one from Europe to Alaska via Siberia and the other from the North Pacific to Alaska (see the vectors in figure 6).

3.3. Regression analysis with the scandinavian pattern index

We further performed an independent regression analysis with the same three meteorological variables used in figure 5. Here we use the Scandinavian pattern index; a known climate pattern originally referred to as the Eurasia-1 pattern (Barnston and Livezey 1987). The index is valid for assessing unusual climate such as blocking, temperature anomalies, etc, over Eurasia from Scandinavia to East Eurasia (www.cpc.ncep.noaa.gov/data/teledoc/scand.shtml). Regression maps between the sign-reversed July and August mean Scandinavian pattern index and the three meteorological variables (figure 7) show a very similar climate pattern in the atmosphere obtained from the composite differences (figure 5). Positive anticyclonic anomalies at 850 and 500 hPa over Europe, Siberia, and subpolar North America (Alaska and Canada) were evident, corresponding to the near-surface warm anomalies (figures 5 and 7). These relationships imply that the climate pattern that characterizes the 13 highest $PM_{2.5}$ summer months in the Arctic by the composite analysis (figure 5) is well explained by the inter-annual variations of the sign-reversed July and August mean Scandinavian pattern index for the 2003–2017 period. To emphasize the characteristic of pressure anomalies aligned zonally around the Arctic

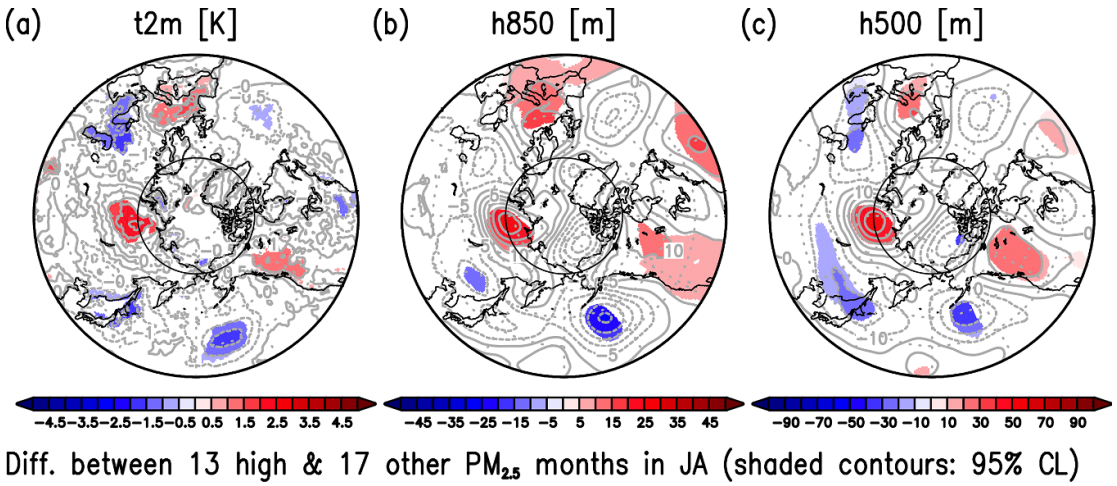

Figure 5. Composited differences (solid contours) in (a) surface air temperature (0.5 K intervals) and (b) geopotential height at 850 hPa (5 m intervals) and (c) 500 hPa (10 m intervals) between the 13 summer months (July and August) of 20 months with the highest $PM_{2.5}$ concentrations in the Arctic region, and the 17 other summer months. Local anomalies that exceed the 95% confidence level based on Welch's t-test (two-sided; see section 2.2) are shown in shaded contours.

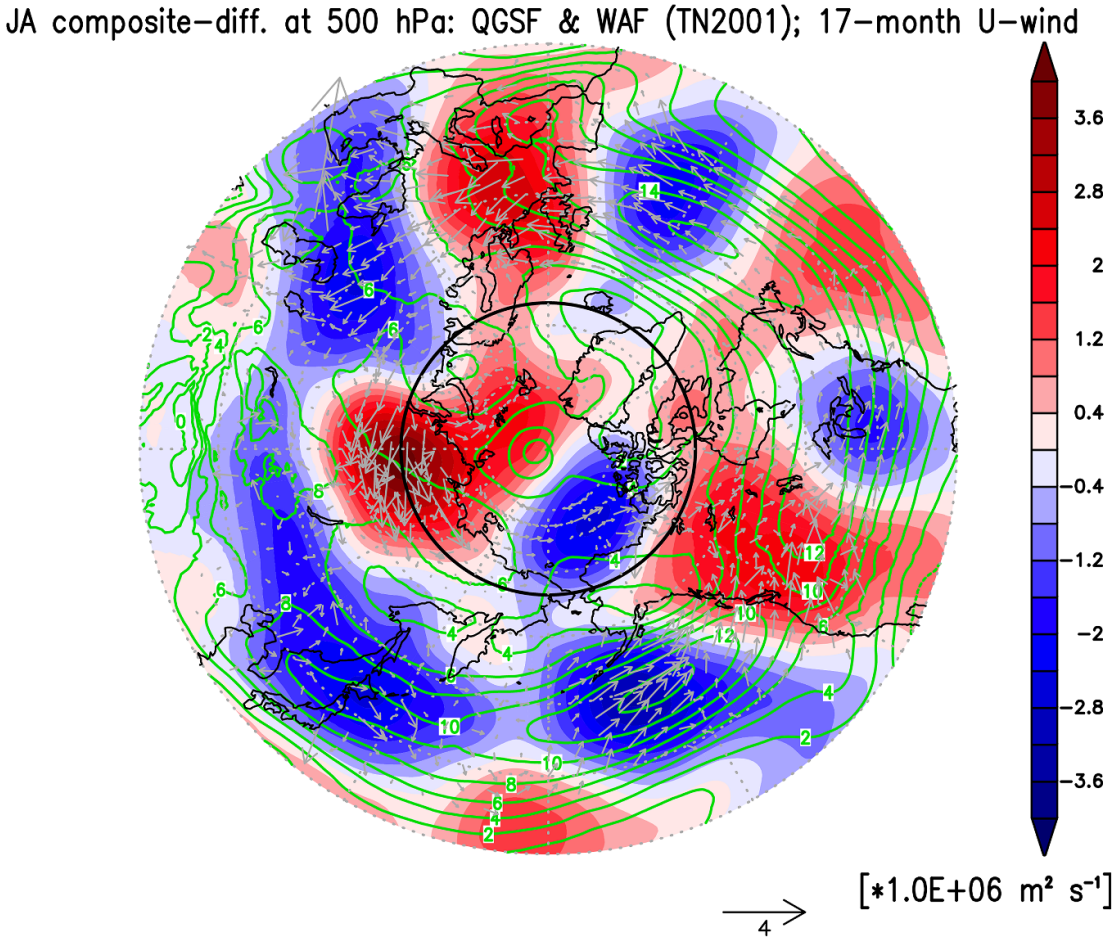

Figure 6. WAF calculated by Takaya and Nakamura (2001) and quasi-geostrophic stream function (shaded contour; see the color bar with the unit shown in the figure) of the composite difference among the 13 summer months of the 20 months with the highest $PM_{2.5}$ and the other 17 summer months (i.e. low $PM_{2.5}$), and the composite of U-wind for the 17 other summer months under the basic $PM_{2.5}$ state (westerly wind in green contour at 1 m s^{-1} interval) at 500 hPa. For WAF (vector in the unit of m^2 s^{-2}), data are plotted at every ten (north of 60° N) and eight (south of 60° N) grid points in the meridional direction, and every five grid points in a longitudinal direction. Besides, we only considered the magnitudes of the basic state of UV-wind equal to or greater than 5 m s^{-1} for plotting the WAF.

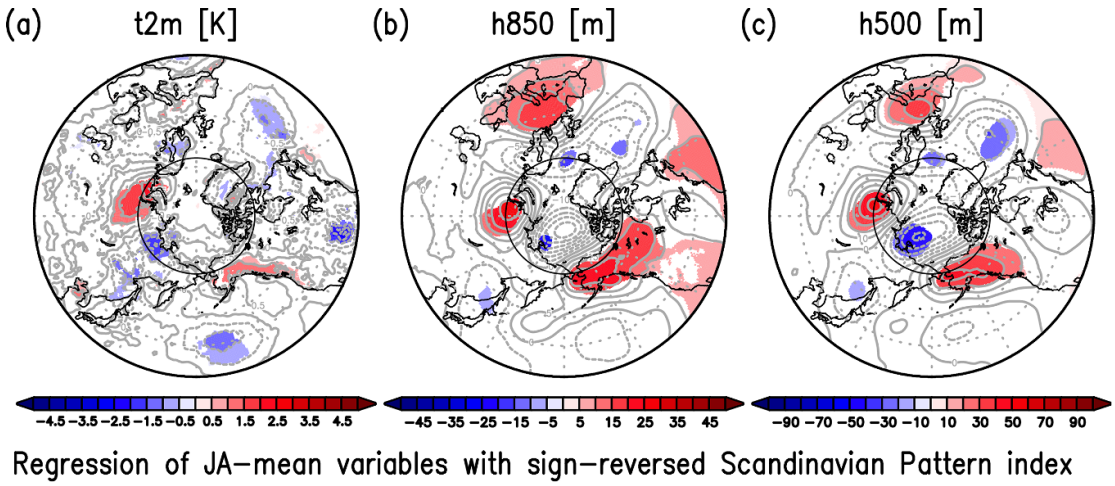

Figure 7. Mean anomalies (solid contours) of July and August (a) surface air temperature (0.5 K intervals), (b) geopotential height at 850 hPa (5 m intervals), and (c) 500 hPa (10 m intervals) regressed against the sign-reversed July and August mean Scandinavian pattern index (see section 2.1). Local anomalies that exceed the 95% confidence level based on t-test (two-sided; see section 2.2) are shown in shaded contours.

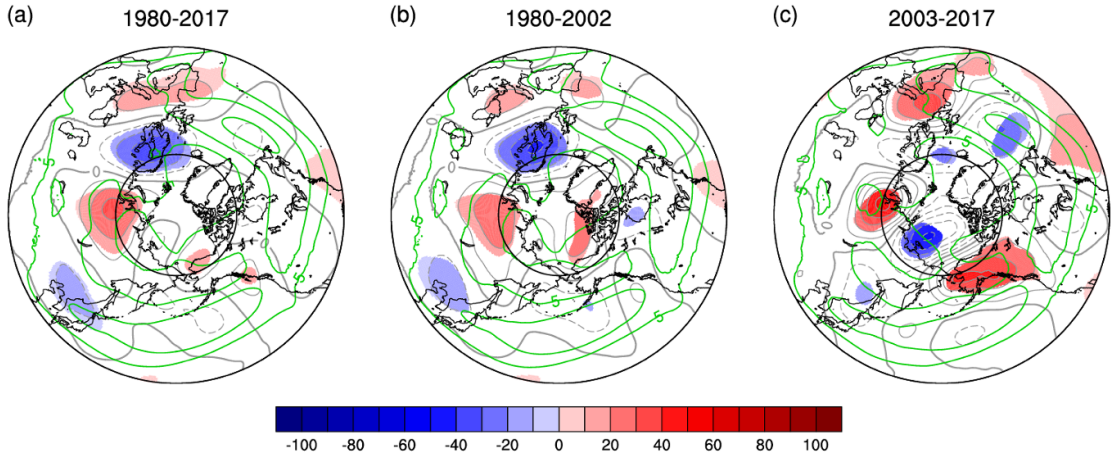

Figure 8. 'Negative' Scandinavian pattern teleconnection pattern for (a) 1980–2017, (b) 1980–2002, and (c) 2003–2017 obtained from the regression of 500 hPa geopotential height anomalies (July and August means) onto the 'negative' (sign-reversed) Scandinavian pattern index. The solid green line denotes the U-wind climatology (i.e. westerly wind) at 500 hPa for each period (plots starting from 5 m s^{-1} with a 5 m s^{-1} interval). Shaded areas indicate 95% statistical confidence.

from Europe to Siberia, Alaska, Canada, and back to Europe, we refer to this summertime climate pattern as the circum-Arctic wave (CAW) pattern.

However, if we performed the same regression analysis extended for a long-term period (i.e. including 1980–2002), the climate pattern only shows a NW–SE oriented (line-shaped) atmospheric teleconnection pattern from Scandinavia to East Asia (figure 8(b)) rather than the CAW. This pattern resembles a typical Scandinavian pattern, as reported in Bueh and Nakamura (2007), although they excluded the summer season from their analysis. This climate pattern exclusively identified over Eurasia is also dominant in the regression for the whole period (1980–2017; figure 8(a)). This characteristic indicates that the typical Scandinavian pattern was dominant over Eurasia before 2003, and afterward, the climate pattern has somehow been modified into forming the CAW. The CAW-associated positive anticyclonic (geopotential height) anomalies at 500 hPa over Europe and Siberia are also stronger than their counterpart associated with the Scandinavian pattern before 2003. This change would imply a possible shift of the summertime climate pattern (teleconnection pattern; i.e. climate links between remote regions) before and after 2003 and forming the co-occurrence of warm surface anomalies over Europe, Siberia, Alaska, and Canada in CAW (figures 5 and 7).

4. Discussion and conclusions

We have found high $PM_{2.5}$ mass concentrations over the summertime Arctic in 2003–2017 (figure 1). These high $PM_{2.5}$ months also correspond to higher POM (figure 2) and its significant increase over Siberia and Canada (SI figures S1 and S2; POM in

Alaska only significant in July: SI table S1), where wildfires were very active (figure 4). OC (also BC) is a good indicator of wildfire activity (BB; e.g. Bond *et al* 2004, Spracklen *et al* 2007, Noguchi *et al* 2015, Yasunari *et al* 2018, Shikwambana 2019). Therefore, we argue that the significantly increasing contributions of organic aerosols to Arctic $PM_{2.5}$ are mainly due to wildfire smoke in and around the Arctic. This characteristic is consistent with results modeled from October 1999 to May 2005 in a previous study (Stohl 2006). In conclusion, for 2003–2017, the 13 higher $PM_{2.5}$ months out of the 20 worst air quality months in the Arctic are explained by the greatly increased OC (POM) with some BC increases from active wildfires in Siberia, Alaska, and Canada.

We have also examined the causes for summers when the Arctic air quality worsens with dominant climate patterns. Investigating those climatic patterns involved in forming warm anticyclonic anomalies over Siberia, Alaska, and Canada under the high $PM_{2.5}$ conditions (i.e. worse air quality) in the Arctic is essential for better prediction of large-scale wildfire occurrences in the future. For this purpose, composite and regression analyses for 2003–2017 were performed (figures 5 and 7). The composite analysis extracted anticyclonic anomalies from the lower to mid-troposphere over Europe, Siberia, and Canada (figures 5(b) and (c)), which locally caused anomalous near-surface warmth and dryness from near the surface to the lower troposphere (figure 5(a); SI figure S3). A recent study with the MODIS fire and MERRA reanalysis (the former product of MERRA-2) data concluded that the primary months of wildfire activity in the circumpolar Arctic tundra region were July and August, and those occurred under warm and dry conditions (Masrur *et al* 2018). Their results strongly support our results. The extreme anomalous warmth is also likely to induce heatwaves (Chase *et al* 2006, Feudale and Shukla 2011); the associated abnormal dryness favors active wildfires (Bondur 2011). Our composited climate pattern in summer (figure 5) is likely to set a favorable condition for heatwaves over Europe and active wildfires (figure 4) over Siberia, Alaska, and Canada, causing high $PM_{2.5}$ and POM and BC emissions in and around the Arctic.

To elucidate the relationship between the climate patterns of recent years (2013–2017) and the long-term, we focused on the Scandinavian pattern as a well-known climate pattern. A recent paper also reported that the Scandinavian pattern is relevant to the summer heatwave activity after the mid-1990s (Choi *et al* 2020), substantiating this index's usefulness for our analysis. As illustrated in the regression patterns in figure 7, the negative phase (i.e. sign-reversed index) of the Scandinavian pattern is characterized by mid-tropospheric anticyclonic anomalies in Europe, central Siberia, Alaska, and Canada. Unlike its counterpart in the cold season (Bueh and Nakamura 2007), the recent summertime Scandinavian pattern or CAW (figure 7(c)) accompanies anticyclonic anomalies from Europe to Alaska along the subpolar westerly jet stream that forms in July and August along the Siberian coast (Nakamura and Fukamachi 2004, Tachibana *et al* 2004). Notably, a similar anomaly pattern, which slightly shifted westward from the corresponding regression patterns (figure 7), is also apparent in the pressure anomalies composited for the 13 summer months with the high $PM_{2.5}$ (figure 5). As demonstrated by the WAF in the atmosphere (figure 6; Takaya and Nakamura 2001), the CAW is likely a manifestation of eastward group-velocity propagation of a stationary Rossby wave train from Europe to Alaska along the upper-troposphere westerly jet stream. The CAW is also associated with near-surface warm and tropospheric dry anomalies, as shown in figure 7(a) and SI figure S3. Our analysis substantiates the previously discussed importance of mid-tropospheric anticyclonic circulations in wildfire occurrences in Siberia and Alaska (Hayasaka *et al* 2016, 2019, Bondur *et al* 2020). Note that the similarity between figures 5 and 7 was unexpected.

A similar eastward-extending Rossby wavy pattern along the subpolar jet stream was observed in summer 2010, which induced extreme warmness, especially in eastern Europe, Russia, and Japan (Otomi *et al* 2013). The particular wave train and that associated the CAW both form along the subpolar jet stream over northern Eurasia in association with the enhanced poleward temperature gradient in summer between the warmer Eurasian continent and the cooler Arctic (Serreze *et al* 2001, Nakamura and Fukamachi 2004, Tachibana *et al* 2010).

Interestingly, the CAW and associated anticyclonic anomalies over Europe, Siberia, and subpolar North America became prominent only from 2003 (figure 8). Amplified anomalies in recent years over Alaska and western Canada can be explained by converging WAF. Those were associated with the wave trains (the one from Siberia via the Arctic Ocean; the other from the North Pacific) if the composite difference pattern in figure 5 and the 'negative' Scandinavian pattern in figure 7 have a similar mechanism (figure 6). Elucidating the CAW formation is beyond the scope of this work but should focus on future studies. A recent numerical simulation showed that a response to a heat source prescribed in western Russia could be similar to the Scandinavian pattern over Siberia (Choi *et al* 2020). Their results may explain the summer CAW observed in the recent years (figure 7(c)), resulting in co-occurrences of heatwaves over Europe and large-scale wildfires in Siberia and subpolar North America, notably Alaska and Canada (figures 4, 5(a) and 7(a)).

Therefore, it is not surprising to observe a quasi-stationary wave train in late June 2019, similar to the CAW as a recent example (SI figure S4). This situation

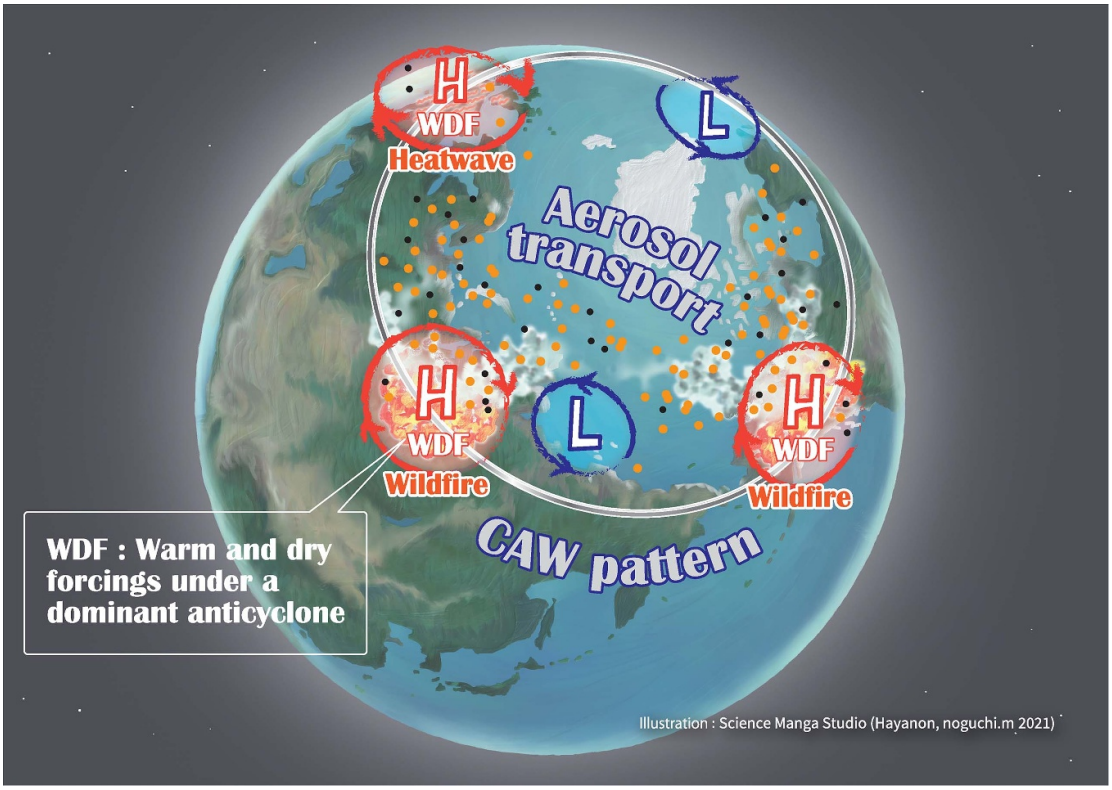

Figure 9. Schematic summary of the results obtained in this study. Anomalous anticyclones developed concomitantly in summer (July and August) over the circumpolar regions: Europe, Siberia, and subpolar North America (i.e. Alaska and Canada). Those anticyclones induce warm and dry forcings from the surface to the mid-troposphere. This study names this climate pattern the CAW pattern. Those anomalous anticyclones induce heatwaves over Europe and active wildfires over Siberia and subpolar North America. The wildfire smoke emitted OC and BC aerosols into the atmosphere, and those aerosols could reach the Arctic region to increase $PM_{2.5}$ there. The interactions between the CAW pattern and the atmospheric aerosols must be investigated in future studies. Reproduced from Hayanon Science Manga Studio. CC BY 3.0.

likely induced the concomitant occurrence of a heatwave in Europe, and the Siberian and Alaskan wildfires, as mentioned in section 1. The climatic impacts of the Scandinavian pattern during fall, winter, and spring have been well explored (Blackburn and Hoskins 2001, Bueh and Nakamura 2007, Pall *et al* 2011). However, a recent study (Choi *et al* 2020) and this study have only emphasized the importance of the corresponding summertime pattern on heatwaves and related large-scale wildfires.

A schematic in figure 9 summarizes all the possible connections from the unique circumpolar atmospheric circulation pattern in summer, CAW, which has become predominant since 2003, to highly increased aerosols in the Arctic. The CAW pattern can induce the anomalous warmth (figure 7(a)) and dryness near the surface and in the lower troposphere (figure S3) under anomalous high-pressure systems (figures 7(b) and (c)). The anomalous anticyclones are likely to cause heatwave over Europe and wildfire occurrences in Siberia and subpolar North America (Alaska and Canada) (figure 4) with massive aerosol injections such as POM and BC into the atmosphere (figure 3; SI figures S1 and S2; SI table S1). The CAW-associated atmospheric circulation can eventually transport the wildfire-induced aerosols into the Arctic, acting to lower air quality (figure 2). The interaction between the aerosols and CAW may be possible through the impact of carbonaceous aerosols on climate via radiative effects (e.g. Liu *et al* 2014, Zhang *et al* 2017). However, we have presented no solid evidence to substantiate this interaction. Therefore, further investigation is needed in the future.

Our study reveals the climatic significance of the recent July and August mean Scandinavian pattern, particularly its 'negative phase' (i.e. CAW pattern). As a stationary atmospheric Rossby wave train with fast eastward group velocity (figure 6), the CAW can act as a useful dynamic indicator in summer of the simultaneous occurrences of heatwaves in Europe, Siberia, Alaska, and Canada, and also works to increase the probability of large-scale wildfires in Siberia, Alaska, and Canada, and thereby higher $PM_{2.5}$ and OC (POM) concentrations in the Arctic. A recent study reported the relationships among wildfire activity in the Arctic tundra and meteorological variables (Masrur *et al* 2018). In conjunction with that study, this study further provides perspectives on their connections to wildfire-induced air pollution and spatiotemporal climate pattern. As increasing wildfires projected under global warming have been discussed (Veira *et al* 2016), further investigations are

required to deepen our understanding of the summertime CAW pattern. The trigger mechanism and its persistence under such climate conditions as sea-surface temperature anomalies are yet to be explored. It is also essential to assess whether the CAW will likely emerge throughout the extended summer season under the warming climate. A better projection of this will help take effective measures of large-scale summer heatwaves and severe wildfires that lead to massive air pollutants in and around the Arctic.

Data availability

The data used in this study are available from the corresponding author or co-authors upon reasonable request. MERRA-2 and fire data from MODIS are also publicly available at: https://gmao.gsfc.nasa.gov/reanalysis/MERRA-2/; https://feer.gsfc.nasa.gov/index.php.

The data that support the findings of this study are available upon reasonable request from the authors.

Acknowledgments

We want to thank two anonymous reviewers for their helpful comments in revising the paper. This study is supported in part by the Japanese Ministry of Education, Culture, Sports, Science and Technology through the Arctic Challenge for Sustainability (ArCS; JPMXD1300000000) project and its successor project (ArCS II; JPMXD1420318865), and by the Japan Society for the Promotion of Science through the Grants-in-Aid for Scientific Research (JSPS KAKENHI 17H02958, 17KT0066, 18H01278, 19H01976, 19H05668, 19H05698, 19H05702, 20H01970, and 20K12197) and by the Japanese Ministry of Environment through Environment Research and Technology Development Fund JPMEERF20192004. NASA's Global Modelling and Assimilation Office (GMAO) produced the MERRA-2 reanalysis data, and we also used NCCS for data analyses. We also thank NASA's MODIS team for making the fire pixel count data available. Shunsuke Tei (Forestry and Forest Products Research Institute) provided a helpful discussion of the calculations of $PM_{2.5}$ and aerosol composite differences (statistics). Kazuaki Nishii (Mie University) helped with plotting the WAF with the GrADS script. We want to thank Editage (www.editage.com) for English language editing before the initial submission. We appreciate Science Manga Studio (Hayanon, noguchi.m) to make the schematic figure for summarizing our results.

ORCID iDs

Teppei J Yasunari https://orcid.org/0000-0002-9896-9404
Hisashi Nakamura https://orcid.org/0000-0003-1791-6325
Kyu-Myong Kim https://orcid.org/0000-0002-3857-2085
Nakbin Choi https://orcid.org/0000-0002-8696-5916
Myong-In Lee https://orcid.org/0000-0001-8983-8624
Yoshihiro Tachibana https://orcid.org/0000-0002-9194-3375
Arlindo M da Silva https://orcid.org/0000-0002-3381-4030

References

Aoki T, Kuchiki K, Niwano M, Kodama Y, Hosaka M and Tanaka T 2011 *J. Geophys. Res.* **116** D11114
Barnston A G and Livezey R E 1987 *Mon. Weather Rev.* **115** 1083–126
Blackburn M and Hoskins B J 2001 *Department of Meteorology, University of Reading* (available at: www.met.rdg.ac.uk/~mike/autumn2000/son00_paper9.pdf) (Accessed 2 March 2021)
Bond T C, Streets D G, Yarbe K F, Nelson S M, Woo J-H and Klimont Z 2004 *J. Geophys. Res.* **109** D14203
Bondur V G 2011 *Izv. Atmos. Ocean. Phys.* **47** 1039–48
Bondur V G, Mokhov I I, Voronova O S and Sitnov S A 2020 *Dokl. Earth Sci.* **492** 370–5
Bosilovich M G *et al* 2015 *NASA/TM–2015–104606* vol **43** (available at: https://gmao.gsfc.nasa.gov/pubs/docs/Bosilovich803.pdf) (Accessed 2 March 2021)
Buchard V *et al* 2017 *J. Clim.* **30** 6851–72
Buchard V, Da Silva A M, Randles C A, Colarco P, Ferrare R, Hair J, Hostetler C, Tackett J and Winker D 2016 *Atmos. Environ.* **125** 100–11
Bueh C and Nakamura H 2007 *Q. J. R. Meteorol. Soc.* **133** 2117–31
Chase T N, Wolter K, Pielke R A and Rasool I 2006 *Geophys. Res. Lett.* **33** L23709
Chin M, Ginoux P, Kinne S, Torres O, Holben B N, Duncan B N, Martin R V, Logan J A, Higurashi A and Nakajima T 2002 *J. Atmos. Sci.* **59** 461–83
Chin M, Rood R B, Lin S-J, Müller J-F and Thompson A M 2000 *J. Geophys. Res.* **105** 24671–87
Choi N, Lee M-I, Cha D-H, Lim Y-K and Kim K-M 2020 *J. Clim.* **33** 1505–22
Colarco P, Da Silva A, Chin M and Diehl T 2010 *J. Geophys. Res.* **115** D14207
Darmenov A and Da Silva A 2015 *NASA/TM–2015–104606* vol **38** (available at: https://gmao.gsfc.nasa.gov/pubs/docs/Darmenov796.pdf) (Accessed 2 March 2021)
Eleftheriadis K, Vratolis S and Nyeki S 2009 *Geophys. Res. Lett.* **36** L02809
Feudale L and Shukla J 2011 *Clim. Dyn.* **36** 1691–703
Flanner M G, Zender C S, Hess P G, Mahowald N M, Painter T H, Ramanathan V and Rasch P J 2009 *Atmos. Chem. Phys.* **9** 2481–97
Flanner M G, Zender C S, Randerson J T and Rasch P J 2007 *J. Geophys. Res.* **112** D11202
Ginoux P, Chin M, Tegen I, Prospero J M, Holben B, Dubovik O and Lin S J 2001 *J. Geophys. Res.* **106** 20255–73
Gleason K E, Mcconnell J R, Arienzo M M, Chellman N and Calvin W M 2019 *Nat. Commun.* **10** 2026
Gueymard C A and Yang D 2020 *Atmos. Environ.* **225** 117216
Hayasaka H, Tanaka H L and Bieniek P A 2016 *Polar Sci.* **10** 217–26
Hayasaka H, Yamazaki K and Naito D 2019 *J. Disaster Res.* **14** 641–8

He L, Lin A, Chen X, Zhou H, Zhou Z and He P 2019 *Remote Sens.* **11** 460
Hegg D A, Warren S G, Grenfell T C, Doherty S J, Larson T V and Clarke A D 2009 *Environ. Sci. Technol.* **43** 4016–21
Hock R G *et al* 2019 *IPCC Special Report on the Ocean and Cryosphere in a Changing Climate H-O Pörtner et al* (eds) in press (www.ipcc.ch/srocc/chapter/chapter-2/) (Accessed 2 March 2021)
Ikeda K and Tanimoto H 2015 *Environ. Res. Lett.* **10** 105001
Jolly W M, Cochrane M A, Freeborn P H, Holden Z A, Brown T J, Williamson G J and Bowman D M J S 2015 *Nat. Commun.* **6** 7537
Keegan K M, Alber M R, Mcconnell J R and Baker I 2014 *Proc. Natl Acad. Sci. USA* **111** 7964–7
Lau W K M, Sang J, Kim M K, Kim K M, Koster R D and Yasunari T J 2018 *J. Geophys. Res.* **123** 8441–61
Liu Y, Goodrick S and Heilman W 2014 *For. Ecol. Manage.* **317** 80–96
Ma J, Xu J and Qu Y 2020 *Atmos. Environ.* **237** 117666
Masrur A, Petrov A N and DeGroote J 2018 *Environ. Res. Lett.* **13** 014019
Nakamura H and Fukamachi T 2004 *Q. J. R. Meteorol. Soc.* **130** 1213–33
Nature 2019 *Nature* **572** 10–1
Noguchi I, Akiyama M, Suzuki H and Yamaguchi T 2015 *Abstract for the 2nd Atmospheric Aerosol Symp. from Kosa to $PM_{2.5}$—Environmental and Health Impacts* p 2 (in Japanese)
Otomi Y, Tachibana Y and Nakamura T 2013 *Clim. Dyn.* **40** 1939–47
Pall P, Aina T, Stone D A, Stott P A, Nozawa T, Hilberts A G J, Lohmann D and Allen M R 2011 *Nature* **470** 382–5
Qian Y, Yasunari T J, Doherty S J, Flanner M G, Lau W K M, Ming J, Wang H, Wang M, Warren S G and Zhang R 2015 *Adv. Atmos. Sci.* **32** 64–91
Quinn P K, Shaw G, Andrews E, Dutton E G, Ruoho-Airola T and Gong S L 2007 *Tellus* B **59** 99–114
Randles C A *et al* 2017 *J. Clim.* **30** 6823–50
Rienecker M M *et al* 2008 *Technical Report Series on Global Modeling and Data Assimilation* vol **27** (available at: https://gmao.gsfc.nasa.gov/pubs/docs/Rienecker369.pdf) (Accessed 2 March 2021)
Running S W 2006 *Science* **313** 927–92
Serreze M C, Lynch A H and Clark M P 2001 *J. Clim.* **14** 1550–67
Sharma S, Lavoué D, Cachier H, Barrie L A and Gong S L 2004 *J. Geophys. Res.* **109** D15203
Shaw G E 1995 *Bull. Am. Meteorol. Soc.* **76** 2403–13
Shikwambana L 2019 *Remote Sens. Lett.* **10** 373–80
Sitnov S A, Mokhov I I and Likhosherstova A A 2020 *Atmos. Res.* **235** 104763
Spracklen D V, Logan J A, Mickley L J, Park R J, Yevich R, Westerling A L and Jaffe D A 2007 *Geophys. Res. Lett.* **34** L16816
Stohl A 2006 *J. Geophys. Res.* **111** D11306
Sun E, Xu X, Che H, Tang Z, Gui K, An L, Lu C and Shi G 2019 *J. Atmos. Sol.-Terr. Phys.* **186** 8–19
Tachibana Y, Iwamoto T, Ogi M and Watanabe Y 2004 *J. Meteorol. Soc. Japan* **82** 1399–415
Tachibana Y, Nakamura T, Komiya H and Takahashi M 2010 *J. Geophys. Res.* **115** D12125
Takaya K and Nakamura H 2001 *J. Atmos. Sci.* **58** 608–27
Tran H N Q and Mölders N 2011 *Atmos. Res.* **99** 39–49
Veira A, Lasslop G and Kloster S 2016 *J. Geophys. Res.* **121** 3195–223
Wang Q *et al* 2011 *Atmos. Chem. Phys.* **11** 12453–73
Warren S G and Wiscombe W J 1980 *J. Atmos. Sci.* **37** 2734–45
Welch B L 1938 *Biometrika* **29** 350–62
Witze A 2020 *Nature* **585** 336–7
Yasunari T J *et al* 2017 *SOLA* **13** 96–101
Yasunari T J, Bonasoni P, Laj P, Fujita K, Vuillermoz E, Marinoni A, Cristofanelli P, Duchi R, Tartari G and Lau K-M 2010 *Atmos. Chem. Phys.* **10** 6603–15
Yasunari T J, Kim K-M, Da Silva A M, Hayasaki M, Akiyama M and Murao N 2018 *Sci. Rep.* **8** 6413
Yasunari T J, Koster R D, Lau K-M, Aoki T, Sud Y C, Yamazaki T, Motoyoshi H and Kodama Y 2011 *J. Geophys. Res.* **116** D02210
Yasunari T J, Koster R D, Lau W K M and Kim K M 2015 *J. Geophys. Res.* **120** 5485–503
Yasunari T J, Lau K-M, Mahanama S P P, Colarco P R, Da Silva A M D, Aoki T, Aoki K, Murao N, Yamagata S and Kodama Y 2014 *SOLA* **10** 50–6
Yasunari T J, Tan Q, Lau K-M, Bonasoni P, Marinoni A, Laj P, Ménégoz M, Takemura T and Chin M 2013 *Atmos. Environ.* **78** 259–67
Yttri K E, Lund Myhre C, Eckhardt S, Fiebig M, Dye C, Hirdman D, Ström J, Klimont Z and Stohl A 2014 *Atmos. Chem. Phys.* **14** 6427–42
Zhang Y *et al* 2017 *Nat. Geosci.* **10** 486–9
Zhao C and Garrett T J 2015 *Geophys. Res. Lett.* **42** 557–64